Supporting Information

A multifunctional flexible magnetic drive gripper for target manipulation in complex constrained environments

Meiying Zhao[1,2], Ye Tao[2]†, Wenshang Guo[1,2], Zhenyou Ge[1,2], Hanqing Hu[3], Ying Yan[4], Chaoxia Zou[5], Guiyu Wang[3]†, and Yukun Ren[1,2]†

[1] State Key Laboratory of Robotics and System, Harbin Institute of Technology, Harbin 150001, China

[2] School of Mechatronics Engineering, Harbin Institute of Technology, Harbin 150001, China

[3] Colorectal Cancer Surgery Department, The Second Affiliated Hospital of Harbin Medical University, Harbin 150086, China

[4] Department of Oncology, The First Hospital of Harbin, Harbin 150010, China

[5] Department of Biochemistry and Molecular Biology, Harbin Medical University, Harbin 150081, China

†Correspondence: taoyehit@hit.edu.cn; guiywang@hrbmu.edu.cn; rykhit@hit.edu.cn

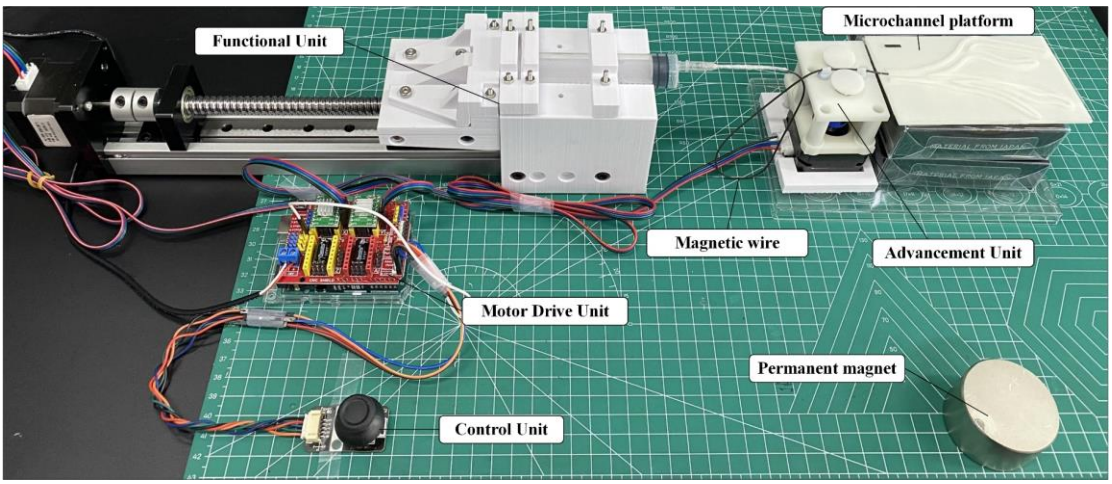

Figure S1. Physical diagram of the experimental auxiliary operating system. The tail end of the magnetic gripper is sealed connected with the syringe of the functional unit, and the syringe is driven to perform suction or injection operations through a screw mechanism. The forward and backward movement of the magnetic gripper in the microchannels is driven by the friction wheel of the advancement unit. The Arduino microcontroller receives signals sent by the joystick and drives the motors of the functional unit and advancement unit through the motor drive board.

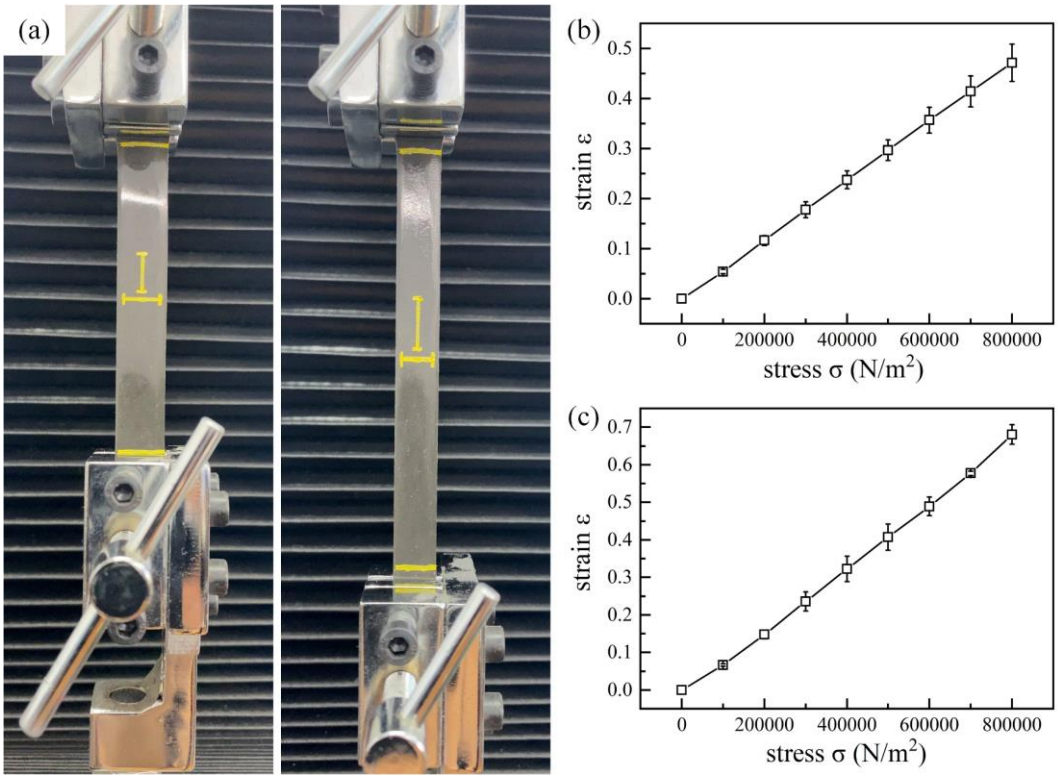

Figure S2. Hollow magnetic wire and auxiliary gripper material testing. (a) Using the same processing procedure as the magnetic gripper, the tensile samples of the magnetic wire and auxiliary gripper are prepared with size: 12 mm × 3 mm × 80 mm. An electronic universal testing machine (WDW-5Y) is used to conduct tensile tests on multiple samples. After data processing, the stress-strain curves of the magnetic wire material and auxiliary gripper material are shown in **(b)** and **(c)** respectively.

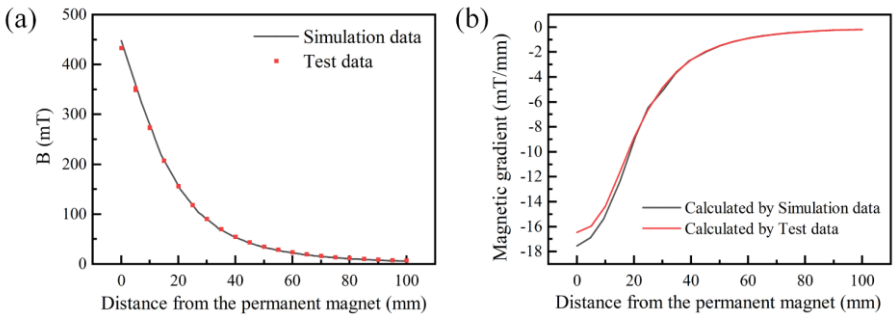

Figure S3. The cylindrical neodymium-iron-boron permanent magnet used in the experiment produces magnetic field properties along the central axis. (a) The simulation and experimental results of the magnetic field strength B at different distances from the extended axis of the permanent magnet. **(b)** The magnetic gradient on the extended axis of the permanent magnet obtained by simulation and test data analysis.

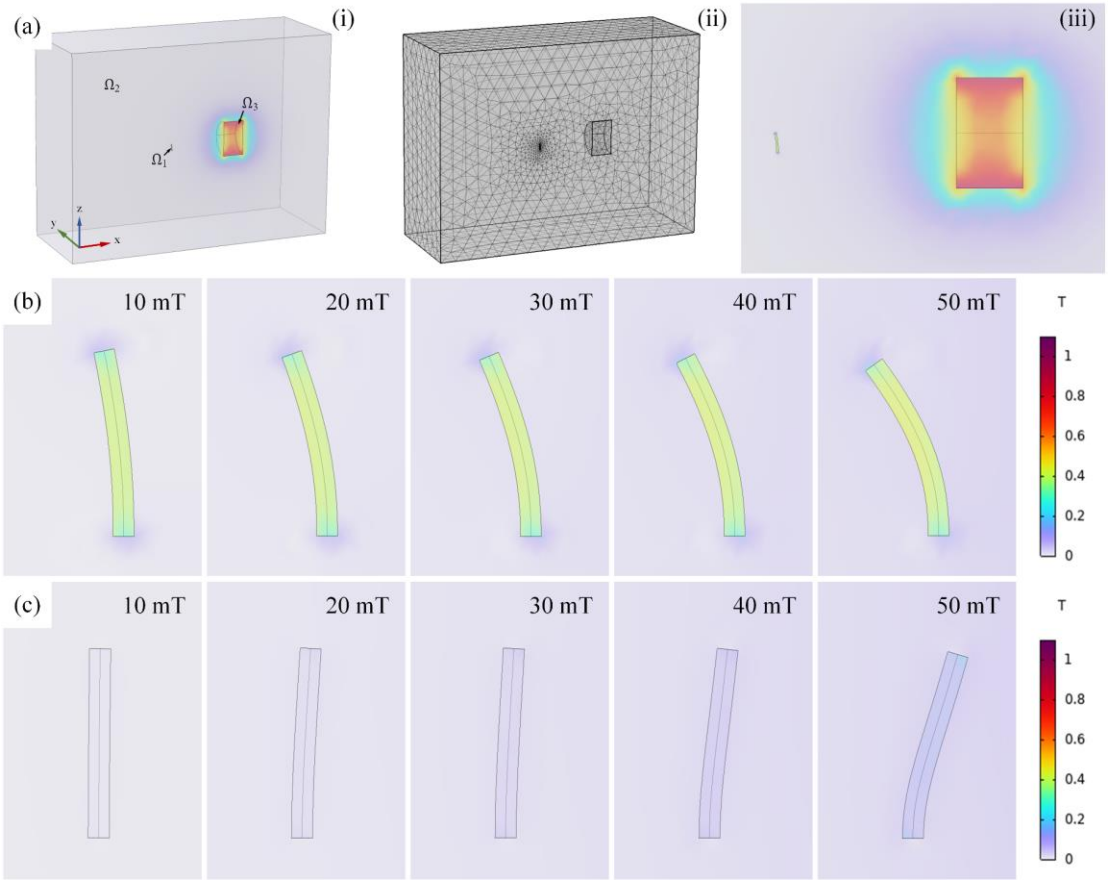

Figure S4. Deformation simulation of unit-sized magnetic drive materials in a non-uniform magnetic field generated by a permanent magnet. (a) Simulation model of the deformation of a unit-sized magnetic drive wire in the spatial static magnetic field generated by a permanent magnet. The model consists three parts: a cylindrical permanent magnet, a unit-diameter magnetic drive wire, and an air domain. The simulation parameters are shown in Table S1. Because of the hard magnetic property of magnetic wire material, set its remanent flux density norm with the direction along the axial direction of the wire; The relative permeability of the auxiliary gripper material is higher than air. The bottom circular surface of the magnetic drive wire is fixed and constrained. The initial endpoint of the magnetic drive wire passes through the extension line of the central axis of the cylindrical permanent magnet. Using the magnetic field intensity generated by the permanent magnet at the free end point of the magnetic wire when the magnetic drive material is undeformed as the reference, the simulation calculates the degree of bending deformation of the unit magnetic drive material under different magnetic field conditions. **(b)** Using unit-sized hollow magnetic wire materials doped with neodymium iron boron particles will bending gradually towards the direction away from the magnet as the magnet approaches. **(c)** Using unit-sized auxiliary gripper materials doped with Fe_3O_4 particles will gradually bend towards the magnet as the magnet approaches.

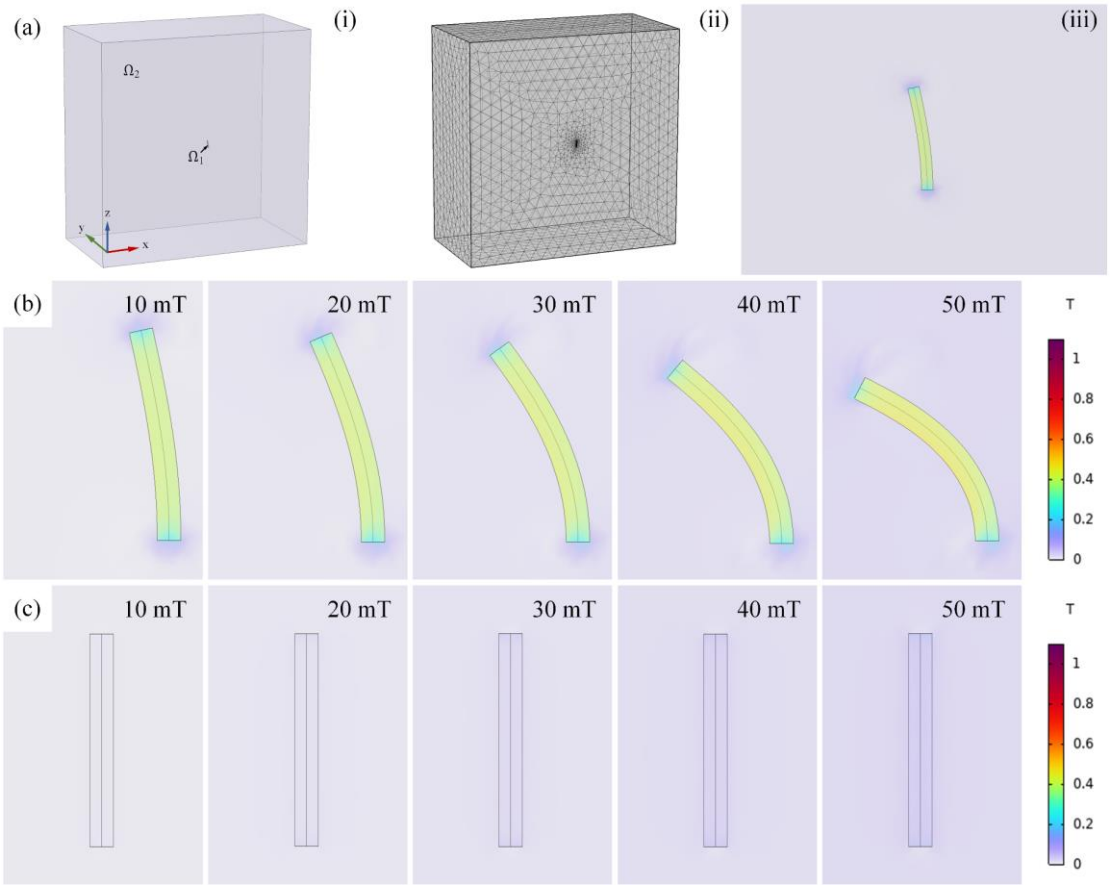

Figure S5. Simulation of deformation of unit-sized magnetic drive materials in a uniform magnetic field. (a) Simulation model of the deformation of a unit-sized magnetic drive wire in the uniform magnetic field. The model consists two parts: a unit-diameter magnetic drive wire, and an air domain. The simulation parameters are shown in Table S1. The bottom circular surface of the magnetic wire with a unit diameter is fixed and constrained. The settings of magnetic drive wires and air domain are consistent with those of the simulation model driven by permanent magnet. The difference is that the magnetic field in space is applied by the outer boundary magnetic flux density of the air domain. **(b)** By using unit-sized hollow magnetic wire materials doped with neodymium iron boron particles, as the magnetic field strengthens, the materials gradually undergo bending deformation due to the action of the magnetic torques. **(c)** Using unit-sized auxiliary gripper materials doped with Fe_3O_4 particles, the simulation model suggests that with the magnetic gradients in a magnetic field being approximately zero, the magnetic drive materials undergo almost no deformation as the uniform magnetic field increases.

Governing Equations and Boundary Conditions for Simulation

Taking the deformation simulation of unit-sized magnetic wire materials in a non-uniform magnetic field generated by a permanent magnet as an example, the governing equations and boundary conditions applied in the simulation are illustrated. Definition: magnetic drive wire (Ω_1), air domain (Ω_2) and cylindrical permanent magnet (Ω_3), as shown in Fig.S4a.

1. In the "Magnetic Fields, No Currents" Model

1.1 Governing Equations

In the simulation, scalar magnetic potential is used to solve the magnetostatic problems without electric currents, where $\boldsymbol{H}$ is the magnetic field intensity, V_m is the scalar magnetic potential and $\boldsymbol{B}$ is the magnetic flux density.

$$\begin{cases} \boldsymbol{H} = -\nabla V_m \\ \nabla \cdot \boldsymbol{B} = 0 \end{cases} \tag{S1}$$

The air domain (Ω_2) and the cylindrical permanent magnet (Ω_3) region only subject to magnetic fields, $\boldsymbol{B}$ is calculated by Eq. S2, where μ_0 is the permeability of vacuum, μ_r is relative permeability and $\boldsymbol{B}_r$ is the remanent flux density. Notably, in the air domain $\boldsymbol{B}_r = 0$.

$$\boldsymbol{B} = \mu_0 \mu_r \boldsymbol{H} + \boldsymbol{B}_r \tag{S2}$$

The magnetic coupling of the magnetic drive wire involves the interaction of magnetic fields and solid mechanics, resulting in significant deformation. Therefore, the magnetic flux density $\boldsymbol{B}$ in domain Ω_1 is obtained by the electromagnetic energy W_{EM} in Magnetic Forces interface.

$$\boldsymbol{B} = -\frac{\partial W_{EM}}{\partial \boldsymbol{H}} \tag{S3}$$

The initial directions of remanent flux density of magnetic wire (Ω_1) and permanent magnet (Ω_3) are $(0,0,1)^T$ and $(-1,0,0)^T$ respectively.

1.2 Boundary Conditions

Due to the symmetry of model, there are boundary conditions (Eq. S4) at the plane of symmetry, where $\boldsymbol{n}$ is the normal vector.

$$\boldsymbol{n} \cdot \boldsymbol{H} = 0 \tag{S4}$$

2. In the "Solid Mechanics" Model

2.1 Governing Equations

The solid mechanics only operates in Ω_1. The governing equations under steady-state conditions are as follows:

$$\begin{cases} 0 = \nabla \cdot (FS)^T + \boldsymbol{F}_V \\ F = I + \nabla \boldsymbol{u} \end{cases} \tag{S5}$$

where $\boldsymbol{F}_V$ is the body force, F is the deformation gradient, I is the identity matrix and $\boldsymbol{u}$ is the displacement field. The second Piola-Kirchhoff stress tensor S is calculated by W_{EM} in Magnetic Forces interface.

$$S = 2\frac{\partial W_{EM}}{\partial C} \tag{S6}$$

The C is right Cauchy-Green deformation tensor.

$$C = F^T F \tag{S7}$$

2.2 Boundary Conditions

In the plane of symmetry,

$$\boldsymbol{u} \cdot \boldsymbol{n} = 0 \tag{S8}$$

The bottom plane of the magnetic drive wire uses a fixed constraint,

$$\boldsymbol{u} = 0 \tag{S9}$$

3. In the "Magnetic Forces" Interface

Under the action of magnetic force, the magnetic drive wire has large deformation. The relationship between magnetic field and solid mechanics as follows:

$$W_{EM} = W_S(C) - \frac{1}{2}\mu_0\mu_r J C^{-1} : (\boldsymbol{H} \otimes \boldsymbol{H}) \tag{S10}$$

where the mechanical energy function $W_S(C)$ depends on the solid model, and $J = \det(F)$ represents the volume change caused by deformation.

Table S1. Simulation parameters for unit-sized magnetic drive materials

Simulation parameter	**Value**	**Unit**
Permanent magnet radius	25	mm
Permanent magnet high	30	mm
Flexible unit magnetic drive material diameter	1	mm
Flexible unit magnetic drive material length	9	mm
Density of hollow magnetic wire materials	1882	kg/m^3
Young's modulus of hollow magnetic wire materials	1700	kPa
Poisson's ratio of hollow magnetic wire materials	0.47	1
Remanent flux density norm of magnetic wire materials	400	mT
Density of auxiliary gripper materials	1542	kg/m^3
Young's modulus of auxiliary gripper materials	1000	kPa
Poisson's ratio of auxiliary gripper materials	0.43	1
Relative permeability of auxiliary gripper materials	4	1

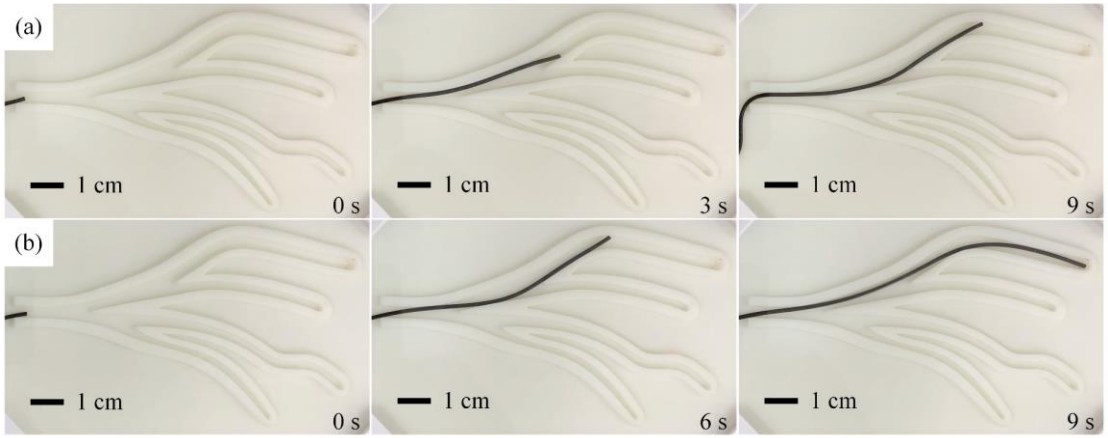

Figure S6. Test of the effect of hollow magnetic wire inner spring on its travel in constrained space. (a) The hollow magnetic wire without internal spring bending at the tail end while passing through a larger bending angle of channel, resulting in insufficient support force and thus unable to achieve flexible guidance in complex constrained spaces. **(b)** Under the same experimental conditions, the hollow magnetic wire with internal spring demonstrated higher support stiffness and was able to smoothly reach the end of the experimental platform.

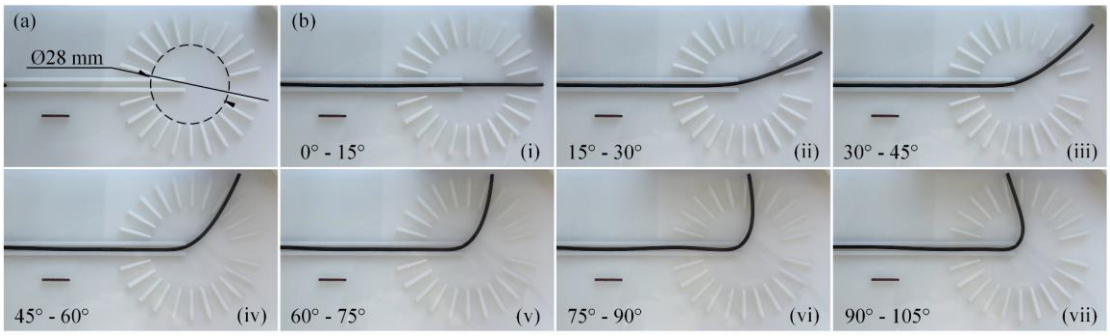

Figure S7. Bending test of hollow magnetic wire under magnetic guidance. (a) The hollow magnetic wire bending test platform. **(b)** The hollow magnetic wire's maximum turning capability allows it to enter channel with angles between 90° and 105°. Due to the negative angle between its forward direction and the pushing force at the tail end of the magnetic wire, in the absence of other sidewalls for support, there is only a certain probability that the hollow magnetic wire can enter the channel and proceed. Within the range of 0° to 90°, the hollow magnetic wire can always smoothly enter the target turning channel by magnetic guidance and the pushing force at the supporting end. All scale bars: 1 cm

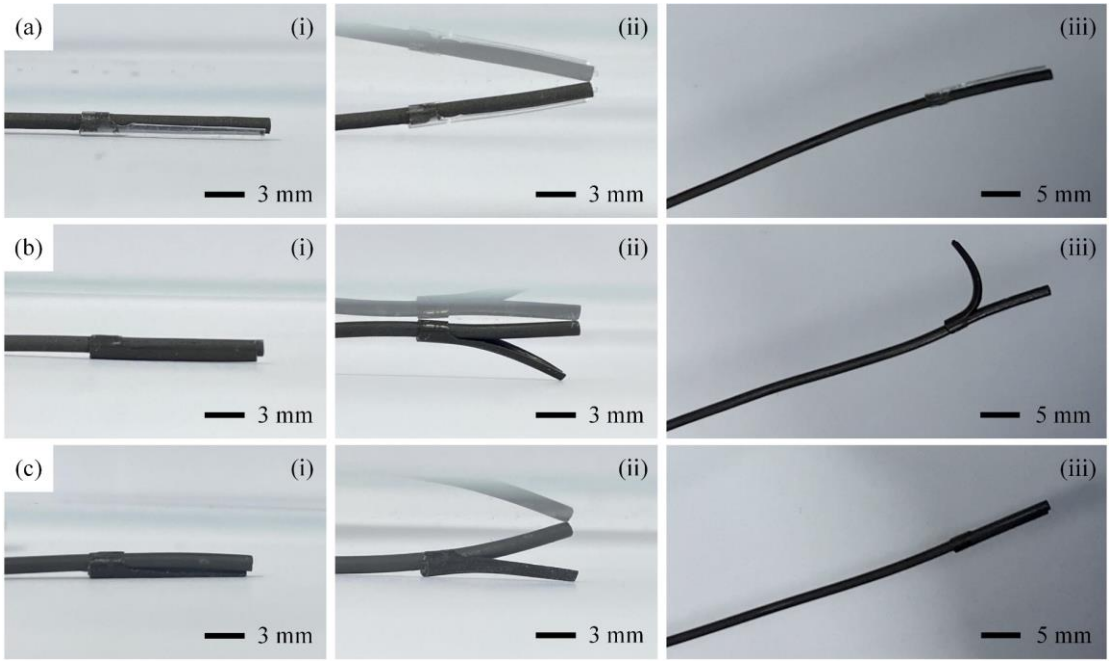

Figure S8. The magnetic actuation of magnetic drive grippers with auxiliary grippers doped with different materials in constrained spaces are compared under the following test scenarios: (i) Manipulation the magnetic drive gripper to close in a constrained space. (ii) Manipulation the magnetic drive gripper to open in a constrained space. (iii) Use a permanent magnet to attract and adjust the orientation at the front of magnetic drive grippers. (a) The auxiliary gripper of the magnetic drive gripper is prepared using pure PDMS. **(b)** The auxiliary gripper is prepared by PDMS doped with neodymium iron boron particles. **(c)** The auxiliary gripper of the magnetic drive gripper is prepared by PDMS doped with Fe_3O_4 particles.

Description of Additional Supplementary File

Supplementary Movie 1 Active guidance of hollow magnetic wire in a 2D drying constrained environment

This video shows a hollow magnetic wire actively choosing its path and sequentially passing through four channels in the experimental platform horizontally under the action of an external magnetic field.

Supplementary Movie 2 Using negative pressure suction function to manipulate microspheres in 2D drying microchannels

This video shows the magnetic wire entering the microchannel where the microsphere is located, adjusting its end posture near the microsphere to align the central hole of magnetic wire with the target, using the negative pressure to capture the microsphere, and then carrying it away from the experimental platform.

Supplementary Movie 3 Active guidance of hollow magnetic wire in a 3D fluid environment

This video shows the hollow magnetic wire overcoming the effects of water flow and gravity in a flowing liquid environment, achieving remote control active guidance within a constrained space.

Supplementary Movie 4 Target operation of magnetic wire in a 3D fluid environment

This video shows the magnetic wire entering the blind end of the fluid channel, capturing the microsphere and then taking it out from the experimental platform.

Supplementary Movie 5 Injection of liquid in a 3D fluid-constrained environment

This video shows the magnetic wire entering the target microchannel in a liquid environment and injecting red liquid into it.

Supplementary Movie 6 Working cycle of the magnetic drive gripper

This video shows the working cycle of the magnetic drive gripper opening and closing as the permanent magnet change its position, completing the clamping function.

Supplementary Movie 7 Manipulating differently shaped microparticles inside microchannels by a multifunctional flexible magnetic drive gripper

This video shows the magnetic gripper manipulating microsphere and polyhedron microparticle from a complex constrained space through suction and clamping, indicating the ability of magnetic drive gripper for operations on targets of different shapes.

Supplementary Movie 8 Achieving circuit connections in complex constrained spaces through the suction and clamping operations of magnetic drive gripper

This video shows the magnetic drive gripper moving the obstacle to enter the constrained working area, connecting the ends of two wires to complete the circuits, and lighting up the lamp.